Inference of mix in direct-drive implosions on OMEGA[a)]

P. B. Radha,[b)] J. Delettrez, R. Epstein, V. Yu Glebov, R. Keck, R. L. McCrory, P. McKenty, D. D. Meyerhofer,[c)] F. Marshall, S. P. Regan, S. Roberts, T. C. Sangster, W. Seka, S. Skupsky, V. Smalyuk, C. Sorce, C. Stoeckl, J. Soures, R. P. J. Town, and B. Yaakobi
Laboratory for Laser Energetics, University of Rochester, Rochester, New York 14623-1299

J. Frenje, C. K. Li, R. Petrasso, and F. Seguin
Plasma Fusion Center, Massachusetts Institute of Technology, Cambridge, Massachusetts 02139

K. Fletcher, S. Padalino, and C. Freeman
SUNY Geneseo, Geneseo, New York 14454

N. Izumi, R. Lerche, and T. W. Phillips
Lawrence Livermore National Laboratory, Livermore, California 94550

(Received 1 November 2001; accepted 7 January 2002)

Direct-drive implosions on the OMEGA laser [T. R. Boehly, D. L. Brown, R. S. Craxton *et al.*, Opt. Commun. **133**, 495 (1997)] have been diagnosed using a wide range of techniques based on neutrons, charged particles, and x rays. These implosions use full single-beam smoothing (distributed phase plates, 1-THz-bandwidth smoothing by spectral dispersion and polarization smoothing). The beam-to-beam power imbalance is $\leqslant 5\%$. Fuel areal densities close to those in one-dimensional (1-D) simulations are inferred for implosions with calculated convergence ratios ~ 15. The experimental neutron yields are $\sim 35\%$ of 1-D yields. The complementary nature of the experimental observables is exploited to infer fuel shell mix in these implosions. Data suggest that this mix occurs at relatively small scales. Analysis of the experimental observables results in a picture of the core and mix region indicating that nearly 70% of the compressed fuel areal density is unmixed, and about 20% of the compressed shell areal density is in the mixed region. Comparisons of this model with inferred core conditions from argon-doped implosions are also presented. © *2002 American Institute of Physics.* [DOI: 10.1063/1.1459452]

I. INTRODUCTION

In the direct-drive approach to inertial confinement fusion (ICF),[1] a spherical target is illuminated directly with a number of individual laser beams. Degradation in target performance occurs primarily through the Rayleigh-Taylor (RT) instability,[2,3] which is seeded by laser nonuniformity and target imperfections. An ICF target is RT unstable during both the acceleration and deceleration phases of an implosion.[4–6] Laser nonuniformity can result in secular growth for low-order modes ($l \leqslant 10$, seeded primarily from beam-to-beam power imbalance and beam mispointing) and RT growth at the ablation surface for the imprinted higher-order modes (seeded by single beam nonuniformities) during the acceleration phase.[4–6] Techniques to smooth laser irradiation on the target, such as smoothing by spectral dispersion (SSD),[7] distributed phase plates,[8] and polarization smoothing (PS)[9] are employed to reduce the seeds for this instability.[10] In addition to laser nonuniformities, target imperfections at the inner surface of the shell feed out to the ablation surface and add to the existing outer surface nonuniformities. Under extreme conditions, the width of the nonuniformity at the ablation surface can become comparable to the in-flight shell thickness, potentially resulting in shell breakup and compromising target performance. During the deceleration phase, the rear surface of the cold, high-density shell is RT unstable. Any pre-existing roughness on the inner surface and perturbations that feed through from the ablation surface grow, resulting in a mixing of the hot fuel and the cold shell. This mixing can decrease compression through the lateral mass flow induced by the instability and quench fusion yields.

Fuel shell mixing can be a combination of low-order (long-wavelength) mode deformations and higher-order (small-scale) distortions. Since higher-order modes have higher RT growth rates ($\gamma \sim \sqrt{k}$, where γ is the growth rate and k is the wavenumber) than low-order modes, these modes will saturate, entering the nonlinear regime sooner, and potentially becoming turbulent. This turbulence could lead to small-scale fuel shell mixing.

Neutron, charged particle, and x-ray diagnostics have been used on the OMEGA[11] laser system to infer core conditions on gas-filled-plastic-shell direct-drive implosions irradiated by a 1 ns square pulse. Plastic shells are chosen because they offer a wide array of complementary implosion diagnostics. Further, when driven by a 1 ns square pulse, the 20 μm thick plastic shell targets have similar stability during the acceleration phase to those predicted for OMEGA $\alpha = 3$ cryogenic implosions, where α is the adiabat of the main fuel layer.[10,12] The OMEGA cryogenic targets are in turn, energy-scaled surrogates for direct-drive ignition targets.[12–14] One

[a)]Paper QI2 4, Bull. Am. Phys. Soc. **46**, 249 (2001).
[b)]Invited speaker. Electronic mail: radha@lle.rochester.edu
[c)]Also at the Departments of Mechanical Engineering and Physics and Astronomy.

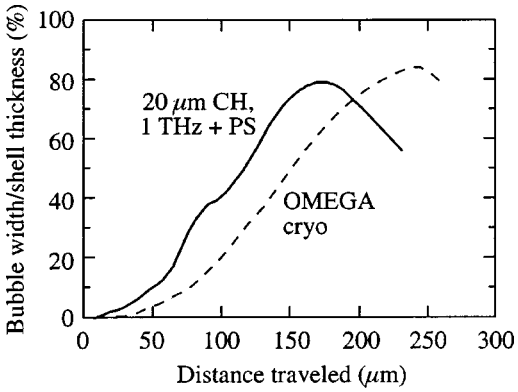

FIG. 1. Ratio of the calculated mix-widths to the in-flight shell thickness for (a) a 20 μm thick plastic shell driven with a 1 ns square pulse with 1 THz SSD and polarization smoothing (PS); (b) for the $\alpha=3$ OMEGA cryogenic target, also with 1 THz SSD and PS.

measure of shell stability is the ratio of the ablation surface mix-widths to the in-flight shell thickness. This ratio is shown in Fig. 1 for the OMEGA $\alpha=3$ cryogenic target and a gas-filled 20 μm plastic-shell target irradiated with a 1 ns square pulse with the full beam smoothing currently employed on OMEGA (2-D SSD with 1 THz bandwidth[7] and PS using birefringent wedges[9]). Figure 1 is an updated version of the figure presented in Ref. 10. The in-flight shell thickness is based on a one-dimensional (1-D) hydrodynamic simulation using LILAC.[15] The mix-thickness is calculated using a Rayleigh–Taylor post-processor (RTPOST).[16] The nonlinear effect of the saturation on mode growth is modeled using the prescription of Haan.[17] The figure indicates that this ratio is very similar for the two implosions indicating similar acceleration phase characteristics.

The instability analysis is also applied to the deceleration phase and indicates that relatively small-scale mixing occurs in these implosions. This is shown in Fig. 2. Figure 2(a) shows the pressure and density profiles from a 1-D simulation of the gas-filled 20 μm plastic-shell target, irradiated with a 1 ns square pulse, at peak neutron production. RT growth occurs when the pressure and density gradients oppose each other. The most RT-unstable region occurs where the steepest gradients of the pressure and density profile occur. However, the experimental signatures of mix occur at the fuel shell interface, which is located 5 μm from the most unstable region located at the inner surface of the shell. The post-processor calculates the feed through of the ablation surface nonuniformities during the acceleration phase to the inner surface of the shell [identified in Fig. 2(a)], which grows during the deceleration phase, yielding the final mode spectrum shown in Fig. 2(b). The cumulative amplitude of the rear-surface nonuniformity above specific l-modes is shown; this amplitude is greater than the distance between the rear-surface in the calculation and the fuel shell interface ($\sim$5 μm). This theoretical analysis indicates that relatively small-scale ($l \geqslant 15$) fuel shell mixing occurs during deceleration in these implosions.

In this paper, we describe a consistent picture of the compressed core and mix based on experiments described in Ref. 10. Arguments for fine-scale mixing are also presented here. The complementary nature of the neutron and charged particle diagnostics and the excellent reproducibility of the OMEGA laser are used to estimate the amount of mixing. Emissivity-averaged core electron density and temperature are compared with the values inferred from x-ray diagnostics.[18]

In Sec. II the targets and laser conditions used to drive these implosions, and the observables are described; mix-dependence of the diagnostics is presented in Sec. III; inference of mix in Sec. IV; and conclusions in Sec. V.

II. TARGETS, LASER CONDITIONS, AND DIAGNOSTICS

The implosions on OMEGA are driven with a 1 ns square pulse with 23 kJ energy. Full-beam smoothing—2-D smoothing by spectral dispersion with 1 THz bandwidth[7] and polarization smoothing using birefringent wedges[9]—is employed to irradiate the targets. Target-shell thickness is kept nominally identical at 19.7 ± 1 μm with a fill pressure of 15 atm. The calculated convergence ratio (CR), which is defined as the ratio of the initial radius of the fuel shell interface to the fuel shell radius at stagnation in a LILAC simulation, is about 15 for this fill pressure. The makeup of the fill gas and details of the shell layers are varied so that complementary diagnostics with differing mix-sensitivities can be applied to each of the fill pressures. The targets comprise plastic (CH)

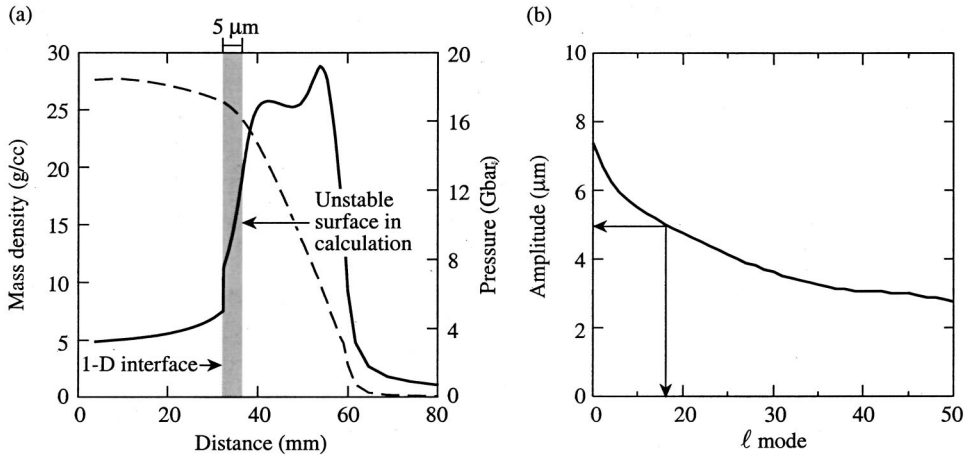

FIG. 2. (a) During shell deceleration, the inner surface of the shell is Rayleigh–Taylor unstable because of the opposite gradients of pressure and density. Shown are the profiles from a 1-D simulation at peak neutron production for a 20 μm thick plastic shell with 15 atm of gas. (b) Post-processed cumulative bubble amplitudes for modes greater than the mode on the horizontal axis for the simulation in (a) shown at peak neutron production. The amplitude of the perturbation is greater than the separation between the fuel shell interface and the unstable interface in the calculation.

TABLE I. The model reproduces many experimental observables with approximately 20% of the compressed shell areal density and 30% of the compressed fuel areal density in the mixed region. An overall burn width of 160 ps is used to obtain yields.

Fill	Shell	Parameter	Measurement	1-D simulation	Model
DT	CH	Fuel ρR (mg/cm^2)	15 ± 3	17	15
D_2	CH	Max: Neutron rate (10^{20}/s)	9 ± 2	48.5	10.1
		D_2 neutron yield (Y_{1n}) (10^{11})	1.5 ± 0.3	4.6	1.76
		T_{ion} (keV)	3.7 ± 0.5	3.1	3.3
		$Y_{2n}/Y_{1n}(10^{-3})$	2.1 ± 0.4	1.75	1.8
		$Y_{2p}/Y_{1n}(10^{-3})$	1.8 ± 0.3	1.9	1.8
^{3}He	CD+CH	T_{ion} (keV)	1.7 ± 0.5	1.3	1.9
		D^{3}He proton yield (10^7)	1.0 ± 0.2	$\sim$0.003[a]	1.0
		D_2 neutron yield (10^8)	4.5 ± 1.5	5.4	6.1

[a]Assumes ^{3}He is initially isobarically diffused throughout the target in the simulation.

shells filled with deuterium (D_2), deuterium–tritium (DT), or argon (Ar)-doped deuterium,[18] and CH shells with embedded deuterated-plastic (CD) layers filled with ^{3}He.

The diagnostic measurements for D_2 targets include primary fusion neutrons, neutron production rates,[19] ion temperature,[20,21] and secondary neutron[22] and proton yields;[23] observables from DT targets include yields and spectra of elastically scattered (''knock-on'') deuterons;[24] the Ar K-shell line emissions from Ar-doped implosions provide a time-resolved diagnostic of emissivity-averaged core electron temperature and density;[18] and ^{3}He-filled targets yield primary D^{3}He protons.[25]

The application of diverse diagnostics across different implosions toward inferring one set of conditions is possible due to the excellent reproducibility of the OMEGA laser.[10] One measure of this reproducibility is the ratio of the experimental yield to the 1-D simulated yield (yield-over-clean or YOC). The mean and standard deviation of this quantity for the CR $\sim$15 targets reported in this paper, obtained over more than 20 different implosions on OMEGA over a one-year period, is $(35\pm5)\%$. The small value of the standard deviation indicates the excellent reproducibility of target conditions in different implosions.

III. MIX SIGNATURES

Mix is indicated by a comparison of measured quantities with those from 1-D LILAC simulations that do not include the effects of mix. Table I shows experimental observables and results from the corresponding no-mix (''clean'') 1-D simulations. The core properties are categorized according to the target gas-fill type and shell constituents and are considered further in the following discussion.

The fuel-areal density is inferred using knock-on deuterons from DT-filled targets.[26] Since these particles are produced by the elastic scattering of the 14-MeV DT neutrons off the background fuel ions, this measurement is insensitive to the location of the fuel and therefore to mix. The mix-insensitive knock-ons indicate experimental fuel areal densities of 15 mg/cm^2, nearly 90% of 1-D values.[24]

Table I also shows that primary DD neutron yields are about 35% of the 1-D simulation. In the unmixed 1-D simulations, most of the neutron yield is produced at a distance that is about two-thirds of the radius of the fuel–shell interface. Therefore, a small amount of mixing can lower temperatures in this region and dilute the density of the fuel, consequently quenching the yield without significantly affecting ρR_f.

Table I shows that the measured value of the secondary to primary neutron ratio is marginally higher than in 1-D simulations $[(2.1\pm0.4)\times10^{-3}$ compared to $1.75\times10^{-3}]$. This ratio increases with increasing mix. Secondary neutrons (Y_{2n}) are produced by the following sequence of reactions:

$$\begin{aligned} &\mathrm{D}+\mathrm{D}\rightarrow T+p, \\ &T+\mathrm{D}\rightarrow\alpha+n(12\text{–}17\ \mathrm{MeV}). \end{aligned} \tag{1}$$

Tritons from the primary DD reaction cause secondary reactions with the fuel deuterons as they move through the target. The ratio of the secondary neutron yield to the primary DD neutron yield (Y_{2n}/Y_{1n}) depends on the compressed fuel areal density (ρR_f).[27–29] However, the secondary neutron ratio is also sensitive to the temperature profile, through the slowing down of the triton and the energy-dependent cross section of the reaction.[29] Since the secondary-reaction cross section increases significantly with decreasing energy of the triton (Fig. 3), this diagnostic is particularly sensitive to the effects of mix; the increased contribution to the electron density from the mixing of the shell material into the fuel en-

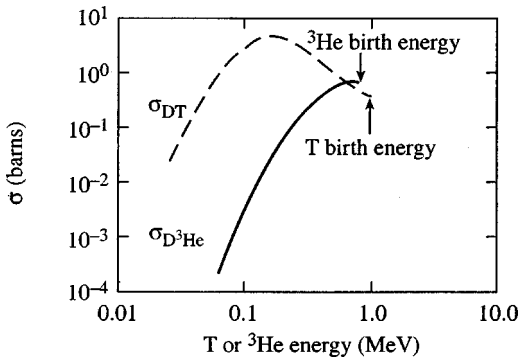

FIG. 3. The cross section of the secondary neutron reaction increases with increasing stopping of the primary tritons whereas the cross section of the secondary proton reaction decreases significantly with increasing stopping of the primary ^{3}He particles.

hances the slowing down of the triton. Consequently the ratio of the secondary neutron yield to the primary neutron yield increases with increasing mix.[29]

To isolate the effect of mix from the effect of the fuel areal density and temperature, a constant density and temperature model is used; any enhancement in the measured secondary neutron ratio relative to this model is directly attributable to mix. The density is specified from the known fuel mass and the experimentally inferred fuel areal density,[24] and the model temperature is the value inferred from Ar-doped implosions.[30] This no-mix model yields a ratio of 1.6×10^{-3} compared to the experimental value of 2.1×10^{-3}; the higher observed value is consistent with mix.

The enhancement in the secondary neutron to primary neutron ratio can, in principle, also occur from a long-wavelength deformation of the core (due to power imbalance or beam mispointing). Tritons produced in the bubbles of the fuel can traverse the shell-spikes before intersecting the fuel again. This would result in additional triton slowing and consequent sampling of a higher fusion cross section with the background deuterons in the fuel. While this would lead to a higher ratio, preliminary calculations on deformed compressed-cores using a two-dimensional Monte Carlo particle tracking approach indicate that this is a small effect ($<10\%$). This is because a small fraction of the total triton yield occurs in the bubbles and an even smaller fraction passes through the fuel twice (from geometric considerations). This leaves small-scale mix as the most likely explanation for the observed enhanced secondary yield.

Secondary protons (Y_{2p}) are produced in an analogous reaction to that of the secondary neutrons. Here, the second main branch of the DD reaction produces primary ^{3}He particles, which in turn fuse with the background deuterons as they traverse the fuel region:

$$\begin{aligned} &\mathrm{D}+\mathrm{D}\rightarrow{}^3\mathrm{He}+n,\\ &{}^3\mathrm{He}+\mathrm{D}\rightarrow\alpha+p(12-17\ \mathrm{MeV}). \end{aligned} \tag{2}$$

The secondary proton to primary neutron ratio (Y_{2p}/Y_{1n}) depends on the fuel areal density and the slowing down of the primary ^{3}He particles. However, unlike secondary neutron reactions, the cross section of this reaction (Fig. 3) decreases significantly with the slowing of the ^{3}He particle after a small initial increase. Consequently, for marginal levels of mixing, the secondary proton ratio will increase with increasing mixing, and for higher levels of mixing this ratio will decrease. Therefore no clear indication of mix is obtained by comparing the secondary proton ratios with 1-D simulation in Table I.

A different measure of mix using secondary particle ratios has been reported in Ref. 29. The ratio of the secondary proton yield to the secondary neutron yield has been shown to have a smaller value with increasing mix. For the implosions considered in this paper, this experimental ratio of ~0.86 is to be compared with the 1-D simulated ratio ~1.1, again indicating mix.

Direct experimental evidence for mixing has been obtained from plastic shells with a 1 μm CD layer at the fuel-shell interface. For ^{3}He targets with an embedded CD layer in the plastic, an observable signal of primary D^{3}He protons can be produced when a significant number of deuterons from the CD layer microscopically mix with the ^{3}He in the fuel. The target fabrication process contaminates the CD layer with a small amount of ^{3}He and thus produces a background to the mix-proton signal. To quantify the effect of this contamination on the proton yield, it is assumed that ^{3}He gas is isobarically diffused throughout the shell. Since ^{3}He does not bind to the plastic molecules in the shell, it is expected that the isobaric assumption represents an upper limit on the amount of ^{3}He. Under these conditions, the initial ratio of D to ^{3}He in the shell is nearly 100:1 resulting in a small yield ($\sim3\times10^4$) during the implosion in a 1-D simulation. The measured yields [$\sim(1\pm0.2)\times10^7$] are more than 300 times higher than the estimated background from 1-D simulation.

The additional observed proton yield can only be obtained by increasing the proportion of ^{3}He relative to deuterium in the CD layer via microscopic mixing during the implosion. One possible source of this difference between the simulated and observed proton yield could be the difference in the temperature and density distributions between simulation and experiment. For instance, a higher proton signal would be expected if the 1-D simulation underestimated the correct ion temperatures. However, it is unlikely that this temperature is significantly in error. The 1-D neutron-averaged ion temperature (1.3 keV) in these implosions (CD layer with ^{3}He fill) is close to the experimental value of 1.7 ± 0.5 keV and additionally the 1-D calculated DD-neutron yield from the CD layer ($\sim5.4\times10^8$) is also close to the measured value of $\sim4.5\times10^8$. This indicates that the density and temperature profiles in the simulation are very close to the experimental profiles. Therefore, any additional measured protons relative to simulation must result from the mixing of ^{3}He into the CD layer during the implosion.

It is also to be noted that the measured yield drops significantly when the CD layer is offset from the fuel-shell interface by 1 μm [the experimental yield is $\sim(7\pm0.1)\times10^5$ compared to $\sim(1\pm0.2)\times10^7$ for the zero-offset case]. This, however, does not necessarily indicate that the mix is due to, at most, 1 μm of initial shell material mixing into the fuel. LILAC simulations indicate that the temperature falls sharply in the shell close to the fuel shell interface. Even if more than 1 μm of initial shell material were to mix in, few additional protons would be produced due to the low temperatures in the outer region of the core-mix region.

IV. MIX ANALYSIS

A static mix model based only on the neutron and particle diagnostics has been constructed to account for the experimental observables reported in Sec. III. The model presented here is a refined version of the model in Ref. 10. This model assumes a clean (unmixed) fuel region and a mixed region consisting of both fuel and shell material (Fig. 4). The mass of the fuel is fixed and corresponds to the initial 15 atm of gas fill, while the mass of the shell in the mix region is varied. The density is assumed to be constant in the clean fuel region and to vary linearly in the mixed region. A Gaussian profile is chosen for the temperature. The electron

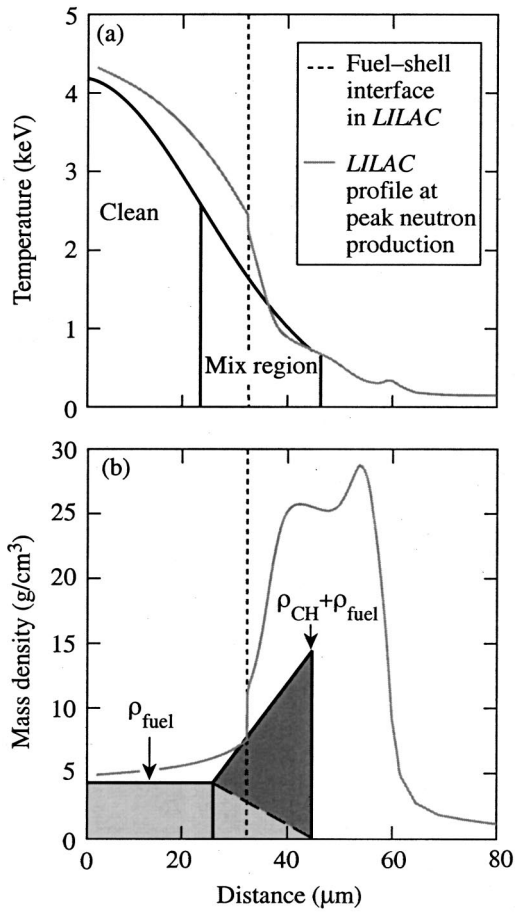

FIG. 4. Shown in (a) are temperature profiles and (b) the density profiles from a mix picture that reproduces data. Also shown are profiles from a 1-D simulation.

and ion temperatures are assumed to be the same because their equilibration time at these conditions is estimated to be about 50 ps, a time scale smaller than the measured duration of neutron production (~170 ps). The model (Fig. 4) is described by six parameters (five free parameters since the mass of the fuel is known): the radius of the clean fuel region, the density of the clean region, the radius of the mixed region, the density of the shell material at the outer edge of the mix region, the temperature of the fuel in the clean region, and the full width at half-maximum of the temperature distribution. The parameters are varied and for each model the secondary neutron and proton yield, the neutron-production rates, and the neutron-averaged ion temperatures are calculated using the Monte Carlo particle tracking code IRIS.[31] This is repeated until good agreement with the experimental data is obtained. The yields from the ^{3}He-filled targets are calculated using the mix profiles determined above and by replacing the D_2 or DT fuel with ^{3}He.

The optimal profiles from these parameters are shown in Fig. 4 together with the corresponding LILAC simulation profiles (ion temperature and mass density) at peak neutron production. In this model, approximately 30% of the fuel areal density is in the mixed region. The shell areal density in the mixed region is about 20% of the compressed shell areal density. (The compressed shell areal density is inferred independently from other diagnostics such as the energy loss of the D^3He proton from the D^3He-filled targets.[32]) The density and temperature profiles compare very well with those from the clean 1-D simulation at peak neutron production, suggesting that these implosions are nearly 1-D in their compression; a small amount of mixing redistributes material near the fuel-shell interface without significantly altering the hydrodynamics of the implosion.

The yields from the model with the optimal profile are compared to experimental observables in Table I. Since the model is static, yields are obtained by the multiplication of the rates in this model by an overall burn width. This burn width (~160 ps) is in good agreement with the measured burn width of (170 ± 20) ps. With five free parameters, the model reproduces nine observables accurately. In particular, the agreement between the calculated D^3He proton mix-yield and the experimental yield is improved by more than two orders of magnitude at this level of mixing.

Finally, a preliminary comparison of the model core conditions with Ar measurements is performed. Time-dependent measurements of Ar K-shell line shapes are made by doping D_2-filled targets with a small amount of argon (~0.05% by atom).[18] This level of Ar doping does not significantly alter the hydrodynamics of the implosion; the neutron yields, secondary neutron ratios, and ion temperatures are similar to undoped targets. Two properties of the optically thin Ar K-shell line shapes (He_β, He_γ, Ly_β) are exploited to infer an emissivity-averaged core electron temperature and density.[18] The line shapes depend strongly on density and are relatively insensitive to electron temperature, whereas the relative intensities of the Ar K-shell lines and their associated satellites are sensitive to variations to electron temperature and density. A value of (1.9 ± 0.2) keV is inferred for the emissivity-averaged electron temperature and $(2.2\pm0.4)\times10^{24}$ cm^{-3} is inferred for the emissivity-averaged electron density from the Ar-doped implosion experiments.[30] Both these values are averaged over the neutron production time in the experiment. The inferred conditions occur at a radius of roughly 31 μm in the mix picture. A more detailed comparison, however, indicates that the corresponding temperature in the model is lower than the inferred value from the Ar-measurements. By replacing the fuel with Ar-doped D_2, the emissivity of the lines is calculated using the non-Local Thermodynamic Equilibrium (non-LTE) radiation model of Ref. 33. These emission profiles are used to calculate the emissivity-averaged core electron temperature and density. The electron densities from the mix picture ($\sim2.7\times10^{24}$ cm^{-3}) marginally agree with the experiment; however, the calculated emissivity-averaged temperature (~1.2 keV) is significantly lower. The Ly_β line, which is the dominant line emission for these conditions, peaks at the outer edge of the mix region. The weighted average of these lines peaks at a radius of approximately 38 μm, not 31 μm used above. The steep temperature gradients in the mix model, consequently, result in the lower emissivity-averaged temperature. This apparent discrepancy reflects the limitation of the mix-model. Ar K-shell spectra are extremely sensitive to electron temperatures in the range of 1–2 keV and the parameters of the static

mix-model have not been tuned to incorporate constraints placed by the Ar measurements.

V. CONCLUSIONS

A detailed analysis of the core and mix region of CR $\sim$15 direct-drive implosions has been performed based on a complementary set of neutron and charged particle diagnostics obtained on OMEGA. Data suggest that mixing on small scales occurs in the experiments. A single set of temperature, density, and material distribution profiles has been inferred across different implosions because of the excellent reproducibility of the OMEGA laser. This static model of the core provides good agreement with the suite of neutron and particle diagnostics. Approximately 30% of the compressed fuel areal density and 20% of the compressed shell areal density in these implosions is in the mixed region. The density and temperature profiles of the core and the mix region obtained from this model are close to those from no-mix 1-D simulations, suggesting that the mixing in these implosions does not significantly alter the 1-D, unmixed hydrodynamics of the implosion. However, only marginal agreement is obtained with these profiles for the conditions inferred from x-ray diagnostics. Rayleigh–Taylor growth from laser imprint and feed through of ablation-surface nonuniformities is one possible source of the inferred small scales. Multidimensional simulations are currently underway to understand and quantify these sources of nonuniformities. A time-dependent mix model[34] is also being developed to further understand the effect of mix on neutron, charged particle, and x-ray diagnostics.

ACKNOWLEDGMENTS

This work was supported by the U.S. Department of Energy (DOE) Office of Inertial Confinement Fusion under Cooperative Agreement No. DE-FC03-92SF19460, the University of Rochester, and the New York State Energy Research and Development Authority. The support of the DOE does not constitute an endorsement by the DOE of the views expressed in this article.

[1] J. Nuckolls, L. Wood, A. Theissen *et al.*, Nature (London) **239**, 139 (1972).
[2] Lord Rayleigh, Proc. London Math. Soc. **XIV**, 170 (1883).
[3] G. Taylor, Proc. R. Soc. London, Ser. A **201**, 192 (1950).
[4] R. Betti, V. N. Goncharov, R. L. McCrory *et al.*, Phys. Plasmas **3**, 2122 (1996).
[5] J. D. Kilkenny, S. G. Glendinning, S. W. Haan *et al.*, Phys. Plasmas **1**, 1379 (1994).
[6] S. E. Bodner, D. G. Colombant, J. H. Gardner *et al.*, Phys. Plasmas **5**, 1901 (1998).
[7] S. Skupsky, R. W. Short, T. Kessler *et al.*, J. Appl. Phys. **66**, 3456 (1989).
[8] T. J. Kessler, Y. Lin, J. J. Armstrong *et al.*, in *Laser Coherence Control: Technology and Applications*, edited by H. T. Powell and T. J. Kessler (SPIE, Bellingham, WA, 1993), Vol. 1870, pp. 95–104.
[9] T. R. Boehly, V. A. Smalyuk, D. D. Meyerhofer *et al.*, J. Appl. Phys. **85**, 3444 (1999).
[10] D. D. Meyerhofer, J. A. Delettrez, R. Epstein *et al.*, Phys. Plasmas **8**, 2251 (2001).
[11] T. R. Boehly, D. L. Brown, R. S. Craxton *et al.*, Opt. Commun. **133**, 495 (1997).
[12] See National Technical Information Service Document No. DOE/SF/19460-344 (Laboratory for Laser Energetics LLE Review, 2000, Vol. 82, p. 49). Copies may be obtained from the National Technical Information Service, Springfield, VA 22161.
[13] C. P. Verdon, Bull. Am. Phys. Soc. **38**, 2010 (1993).
[14] P. W. McKenty, V. N. Goncharov, R. P. J. Town *et al.*, Phys. Plasmas **8**, 2315 (2001).
[15] M. C. Richardson, P. W. McKenty, F. J. Marshall *et al.*, in *Laser Interaction and Related Plasma Phenomena*, edited by H. Hora and G. H. Miley (Plenum, New York, 1986), Vol. 7, pp. 421–448.
[16] V. Goncharov, P. McKenty, S. Skupsky *et al.*, Phys. Plasmas **7**, 5118 (2000).
[17] S. W. Haan, Phys. Rev. A **39**, 5812 (1989).
[18] S. P. Regan, J. A. Delettrez, P. A. Jaanimagi *et al.*, Phys. Plasmas **9**, 1357 (2002).
[19] R. A. Lerche, D. W. Phillion, and G. L. Tietbohl, Rev. Sci. Instrum. **66**, 933 (1995).
[20] T. J. Murphy, R. A. Lerche, C. Bennett *et al.*, Rev. Sci. Instrum. **66**, 930 (1995).
[21] R. A. Lerche and T. J. Murphy, Rev. Sci. Instrum. **63**, 4880 (1992).
[22] V. Yu. Glebov, D. D. Meyerhofer, C. Stoeckl *et al.*, Rev. Sci. Instrum. **72**, 824 (2001).
[23] F. H. Séguin, C. K. Li, D. G. Hicks *et al.*, "Using secondary proton spectra to study imploded D_2-filled capsules at the OMEGA laser facility," submitted to Phys. Plasmas.
[24] C. K. Li, F. H. Séguin, D. G. Hicks *et al.*, Phys. Plasmas **8**, 4902 (2001).
[25] R. Petrasso, C. K. Li, F. H. Séguin *et al.*, Bull. Am. Phys. Soc. **46**, 105 (2001).
[26] S. Skupsky and S. Kacenjar, J. Appl. Phys. **52**, 2608 (1981).
[27] E. G. Gamalii, S. Yu. Gus'kov, O. N. Krokhin *et al.*, JETP Lett. **21**, 70 (1975).
[28] T. E. Blue and D. B. Harris, Nucl. Sci. Eng. **77**, 463 (1981).
[29] H. Azechi, R. O. Stapf, N. Miyanaga *et al.*, Phys. Rev. Lett. **59**, 2635 (1987).
[30] S. P. Regan, J. A. Delettrez, F. J. Marshall *et al.*, "Shell mix in compressed core of spherical implosions," submitted to Phys. Rev. Lett.
[31] See National Technical Information Service Document No. DOE/SF/19460-393 (Laboratory for Laser Energetics LLE Review, 2001, Vol. 86, p. 68). Copies may be obtained from the National Technical Information Service, Springfield, VA 22161.
[32] C. K. Li, D. G. Hicks, F. H. Séguin *et al.*, Phys. Plasmas **7**, 2578 (2000).
[33] R. Epstein, Phys. Fluids B **1**, 214 (1989).
[34] See National Technical Information Service Document No. DOE/SF/19460-99 (Laboratory for Laser Energetics LLE Review, 1995, Vol. 64, p. 160). Copies may be obtained from the National Technical Information Service, Springfield, VA 22161.